How to cite: *Angew. Chem. Int. Ed.* **2022,** *61,* e202206061
International Edition: doi.org/10.1002/anie.202206061
German Edition: doi.org/10.1002/ange.202206061

Soft Matter

# Static and Dynamic Gradient Based Directional Transportation of Neutral Molecules in Swollen Polymer Films

*Mohammad A. Ali,* Brett Volmert, Christopher M. Evans, and Paul V. Braun**

**Abstract:** Materials which selectively transport molecules offer powerful opportunities for concentrating and separating chemical agents. Here, utilizing static and dynamic chemical gradients, transport of molecules within swollen crosslinked polymers is demonstrated. Using an ≈200 μm static hydroxyl to hexyl gradient, the neutral ambipolar nerve agent surrogate diethyl (cyanomethyl)phosphonate (DECP) is directionally transported and concentrated 60-fold within 4 hours. To accelerate transport kinetics, a dynamic gradient (a "travelling wave") is utilized. Here, the non-polar dye pyrene was transported. The dynamic gradient is generated by an ion exchange process triggered by the localized introduction of an aqueous NaCl solution, which converts the gel from hydrophobic to hydrophilic. As the hydrophilic region expands, associated water enters the gel, and pyrene is pushed ahead of the expansion front. The dynamic gradient provides about 10-fold faster transport kinetics than the static gradient.

Biological systems efficiently convert chemical energy into work. For example, proton gradients power adenosine triphosphate (ATP) synthesis, $Na^+/K^+$ gradients drive signal propagation in neurons, and chemical concentration gradients direct cell migration.[1] Though chemists are far from designing such complex systems, synthetic molecular motors,[2] molecular taxis,[3] and chemical gradients[4] have all been shown to drive selective molecular transport along defined pathways. Such systems have received great attention due to their potential to drive formation of nano-scale assemblies,[5] power motion of soft robots,[6] and amplify the signal of chemi/biosensors.[7]

[*] Dr. M. A. Ali, B. Volmert, Prof. C. M. Evans, Prof. P. V. Braun
Department of Materials Science and Engineering, Department of Chemistry, Beckman Institute for Advanced Science and Technology, and Materials Research Laboratory,
University of Illinois Urbana Champaign
Urbana, Illinois 61801 (USA)
E-mail: mali85@illinois.edu
pbraun@illinois.edu



Surfaces containing chemical potential gradients have directed the anisotropic motion of liquid droplets,[8] particles,[9] poly(propyleneimine) dendrimers,[10] poly(ethylene glycol),[11] and adamantine-appended dye molecules.[12] In these examples the species of interest are transported on the surface of a solid. As examples of transport within a material, polyacrylamide hydrogel films containing chemical potential gradients were shown to drive the motion of charged molecules[4c,d] including to small patches of the sample containing nanoantenna-based surface-enhanced infrared absorption sensing elements.[4b,13] In prior work, we also showed how a travelling ionic wave generated through reaction-diffusion processes could drive molecular transport and concentration of charged hydrophilic molecules entrained within a hydrogel, providing enhanced kinetics relative to static chemical gradient assisted directional molecular transport.[4a] Here we now demonstrate directional transportation of neutral molecules (one with and one without attractive interaction to the host-matrix) within swollen crosslinked polymeric films using both static and dynamic gradients.

A static chemical gradient embedded was utilized to transport neutral molecules which exhibit attractive interactions with the functional groups forming the chemical gradient. In the example presented here, the gradient drove a 60-fold concentration of diethyl (cyanomethyl)phosphonate (DECP) within 4 h. Then, using pyrene as an easy to observe example, we show how a neutral molecule without a specific chemical interaction with the gel can be transported via a dynamic chemical gradient (a "chemical wave") formed by a reaction-diffusion (RD) chemistry. Under the influence of the dynamic gradient, pyrene was transported ten times faster than DECP was transported in a static gradient.

The motivation for studying DECP transport is that it contains the diethyl phosphonate group found in many chemical warfare agents and pesticides. The ability to concentrate such a target is attractive for improving the limit of detection of such important compounds. DECP contains the hydrogen bond forming P=O bond,[14] which we suspected would lead to an attractive interaction with hydroxyl groups when the hydroxyl groups are in a low polarity background. We therefore selected a hydroxyl gradient in a solvent-swollen polymer to drive the transport of DECP. We start with a pentafluorophenyl acrylate (PFPA) active ester-derivatized polymer (Supporting Information Section 6.1 and 6.2). This active ester reacts with aliphatic primary and secondary amines to form the corresponding poly(acrylamide) derivatives providing the

 

opportunity to fabricate gradients with varying functionalities.[15] The solvent swelling the polymer is THF; the low polarity of THF relative to water enhances the interactions between the P=O groups and the hydroxyl groups vs. the case if the polymer was swollen with water.

Formation of the static radial gradient starting with the PFPA-derivatized polymers involved two steps (Figure 1a). First, a hydroxyl gradient was formed through localized dosing of an amine-appended hydroxyl compound onto a film of the polymer. Upon localized dosing of this compound, it diffuses radially across the film, creating a radial concentration gradient within the gel as it reacts with active esters in the polymer, becoming appended to the gel backbone with amide bonds (Figure 1b).

The moderate coupling reaction rates (PFPA reacts with hexylamine at a rate of $1.85\times10^{-3}\ s^{-1}$ at 50 °C in THF)[15] at room temperature allows the amine-appended molecule to form a concentration gradient within polymer before significant coupling proceeds. After coupling, the polymer film is transferred to a solution containing an amine-appended hexyl molecule, converting remaining active esters to amide-bonded hexyl groups. The gradient shape can be controlled during the amine-appended hydroxyl molecules coupling reaction step by applying different localized injection approaches (Figure 1b). Note, the polymer films are thin (ca. 4 μm) compared to the lateral gradient dimensions (100–150 μm), and thus, the diffusion is effectively occurring in two dimensions.

To investigate the static gradient transportation behavior, a nominally linear gradient is fabricated (see Supporting Information for fabrication details). The rectangular film contains hydroxyl groups (generated via reaction with 3-aminopropane-1,2-diol) on one end and hexyl groups (generated via reaction with N-methylhexan-1-amine) on the other, with a hydroxyl-to-hexyl gradient in between. The hydroxyl group exhibits a broad peak centered around 3000 $cm^{-1}$, (See Supporting Information 6.5) enabling the quantification of its content at selected locations along the gradient. All Raman spectra are normalized by the C–C stretch of the polymer backbone at ca. 1096 $cm^{-1}$.[16] By integrating the Raman spectra from 1000 $cm^{-1}$ to 3800 $cm^{-1}$ along the gradient, the gradient length is found as ca. 100–150 μm (Figure 1c).

The film containing the linear hydroxyl gradient is then dosed with DECP by spreading a 0.1 mM DECP solution in THF on the film. The DECP cyano group exhibits a distinct stretch peak at ca. 2250 $cm^{-1}$, enabling quantification of its content at selected locations along the gradient. The dosed film is left in the fume hood to evaporate the THF and another Raman line scan along the gradient was performed (once THF is removed, the polymer is glassy, and diffusion of DECP is minimal). The hydroxyl group peak $\nu$(O–H) at 3400 $cm^{-1}$ is plotted against the cyano group and it is observed that DECP is dosed uniformly across the film (Figure 2b). The dosed film is then transferred to a sealed THF vapor saturated chamber, allowing the film to uptake THF, facilitating movement of the DECP. After 5 h, a

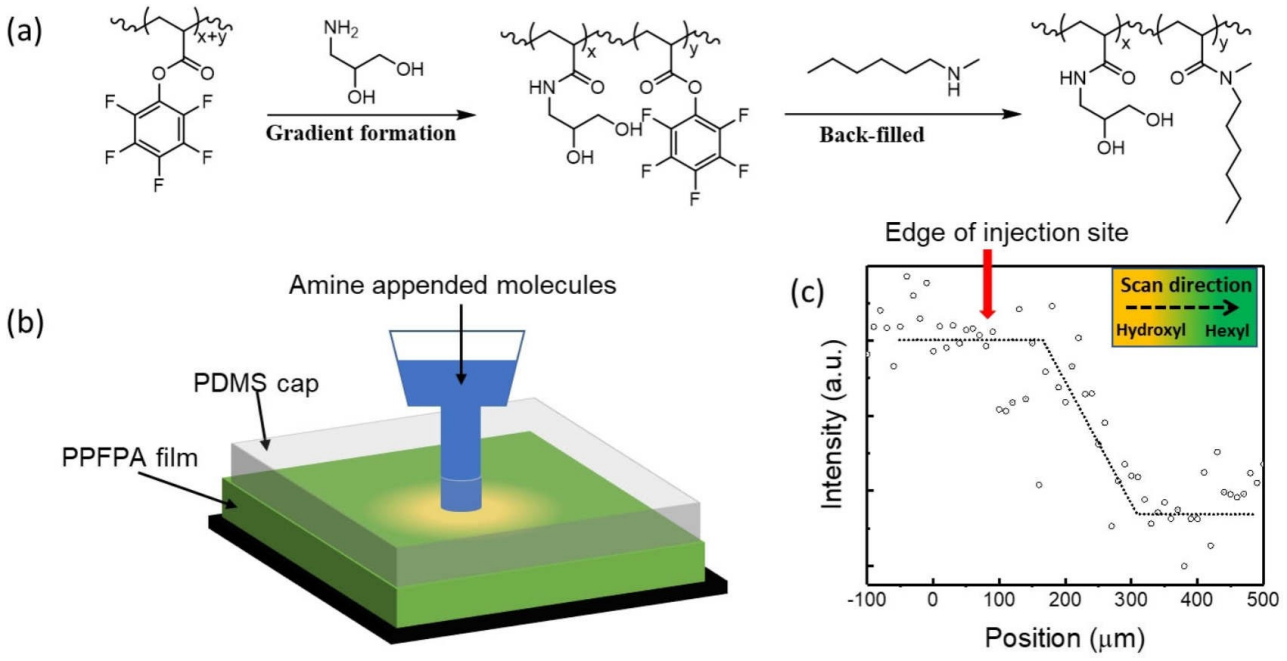


***Figure 1.*** Static chemical gradient formation. a) Synthetic route for appending hydroxyl and hexyl functional groups onto the polymer forming the gradient. $x+y$ represents the molar percentage of pentafluorophenyl repeating units in the pristine polymer. $x$ molar percent of pentafluorophenyl groups were selectively replaced by amine-appended hydroxyl molecules. The remaining ($y$) pentafluorophenyl groups were replaced by amine-appended hexyl molecules. b) Experimental setup for generating a localized chemical reaction to create a radially symmetric chemical gradient in the polymer film. Details of the fabrication process can be found in Supporting Information 6.4. c) Integrated (1000 $cm^{-1}$ to 3800 $cm^{-1}$) Raman intensity along a one-dimensional hydroxyl gradient.

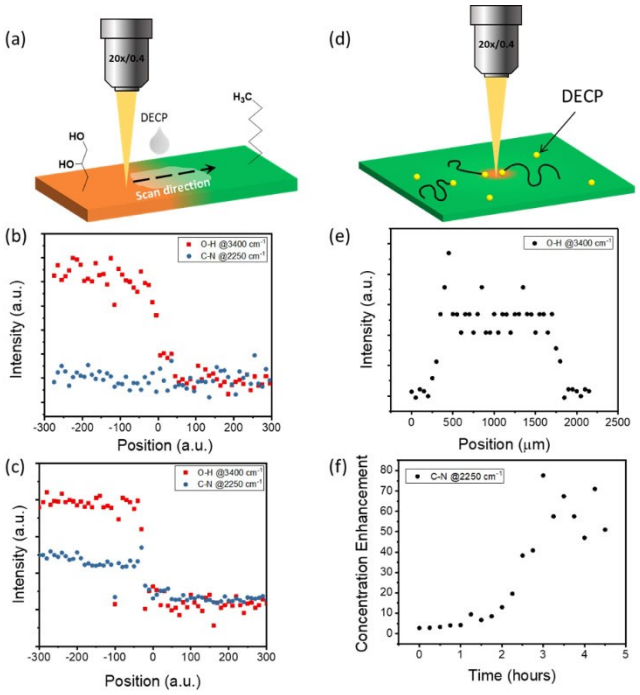


***Figure 2.*** Directional transportation and concentration of non-polar species via chemical gradients. a) Schematic diagram of confocal Raman characterization showing the scan direction of the data acquisition point across the hydroxyl gradient direction. Normalized Raman peak intensities of OH and CN across the gradient, before (b) and after (c) molecular transportation. d) Top-view illustration of confocal Raman characterization showing data acquisition point over time. e) Normalized hydroxyl peak intensity along radially symmetric hydroxyl gradient. f) Concentration enhancement as a function of time. The Raman spectra were normalized by the C–C stretch of the polymer backbone at ca. 1096 $cm^{-1}$.

Raman line scan is performed along the gradient length to quantify the concentration of DECP as a function of position along the gradient.

The concentration of DECP on the hydroxyl functionalized side is significantly greater than the hexyl functionalized side, suggesting DECP is transported towards the hydroxyl functionalized side of the film area by the chemical gradient. We suspect the primary attraction between the hydroxyl group and DECP is due to the P=O bond in DECP, and not the cyano group, as the P=O bond is much more polar (electronegativity difference between P and O is 1.25 eV) than the cyano group (electronegativity difference between N and C is 0.49 eV), however, both groups could be contributing.

To drive molecular concentration by the gradient, the radially symmetric gradient (SI 6.4) is applied. The geometry of the radially symmetric gradient is characterized using confocal Raman spectroscopy (Figure 2e). The radius of the OH-functionalized circular area is ≈1 mm with a 150–200 μm gradient around the periphery. The length of the gradient is comparable with that of the linear gradient. Using an atomizer, a 0.1 mM DECP solution in THF is sprayed on a dry film containing a radially symmetric hydroxyl-to-hexyl gradient and the THF was allowed to evaporate. The dosed film was transferred to a sealed THF vapor saturated chamber, allowing the film to uptake THF, facilitating movement of DECP. Raman spectra are then collected at the center of the radially symmetric gradient as a function of time (Figure 2f). The intensity of the cyano peak increases gradually and then rapidly, until reaching a maximum after about 3 hours. The concentration enhancement is defined as the intensity of the cyano Raman signal divided by the intensity of cyano peak at time 0 h (the as sprayed film). Via this definition, the peak of the concentration enhancement is found to be ca. 60. If the gradient center is a perfect sink, the upper bound of the concentration enhancement can be estimated as the ratio of the total area of the hydrogel film to the area of the gradient center $= A/\pi r^2 = 127$, where $A$ is 4 $cm^2$, the area of the entire film and $r$ is 1 mm, the radius of the roughly uniformly chemically functionalized center of the radially symmetric gradient). We did not investigate the difference between the measured and upper bound of the concentration enhancement given the concentration enhancement was within a factor of 2 of the upper bound. Note, we also investigated the DECP transportation and concentration using a phenolic hydroxylic gradient (formed by dopamine appended molecules rather aliphatic hydroxyls) and a similar result is found. See Supporting Information 6.6.

To transport neutral molecules, which do not have a strong attraction to the host matrix, a dynamic gradient (a "travelling wave") formed by a coupled reaction-diffusion process was utilized. As an example, we apply a dynamic chemical gradient which propagates across the gel, with a steep slope in chemical potential at the front of the gradient (gradient length order of few microns or less), building off our previously published reaction-diffusion (RD) dynamic gradient efforts.[4a] RD chemistries are particularly useful to generate propagating gradients as they use dissipative chemical reactions to drive transport faster than free diffusion. It is worth noting that RD processes are commonplace in natural systems, where they serve to govern the motion of molecules and associated information.[17] To form a synthetic RD system, we start with the quaternary ammonium group-containing polymer poly[2-(methacryloyloxy)ethyl] trimethylammonium (PMTA) which offers a counterion-dependent hydrophobicity. The counterion-dependent properties of this polymer served as the basis for forming a hydrophobic-to-hydrophilic gradient. When water swollen, the equilibrium water content in the polymer decreased from 70 ± 5 w/w% to 38 ± 3 w/w% when counterion is changed from $ClO_4^-$ to $Cl^-$ (Table S2). We note, a similar change in hydrophobicity was also reported for a quaternary ammonium-containing polymer brush as a function of counterion.[18]

In the brush system, the contact angle changed from 79° to 35° when counterion was changed from $ClO_4^-$ to $Cl^-$.[18] Upon investigating the water uptake of the gel for multiple different counterions, the water uptake was observed to follow the trend: $Cl^- < NO_3^- < SCN^- < ClO_4^- < TFSi^-$ (Table S2). Not surprisingly, this trend is very similar to a Hofmeister-type series, which orders ions in order of their

ability to salt out or salt in proteins in aqueous salt solutions.[19]

The $TFSi^-$ ion generates the most hydrophobic gel, but the gel is mechanically brittle. We determined the next ion in the series, the $ClO_4^-$ counter ion, results in a gel that is both mechanically stable and sufficiently solubilized the non-polar molecules of interest. As such, this gel was selected as the starting point to transport non-polar species. To initiate transport, the $ClO_4^-$ counterion is locally exchanged with $Cl^-$ by flowing a solution of NaCl in a 1:1 water:DMSO mixture (by volume) through a microchannel placed on top of the gel film (Figure 3b). The selective binding affinity of the quaternary ammonium group to $Cl^-$ drives the exchange nearly to completion, making the gel considerably more hydrophilic. A simple aqueous NaCl solution was not used as no gradient was observed in that case (Figure 3ci). We suspect the aqueous NaCl solution simply does not penetrate the hydrophobic gel, hence no ion-exchange occurred. Figure 3c includes optical images of the ionic gel at different times after flowing a 2 M NaCl solution through the microchannel. While we do not understand the exact origin of the dark spots in the collapsed polymer (Figure 3ci–iii), they do not appear to modify transport, and disappear as the polymer swells. To increase the gel solvation, the binary water:DMSO solvent mixture was used. Water and DMSO are miscible and NaCl is soluble in both solvents (solubility of NaCl at 25 °C is 359 $g\,L^{-1}$ and 4 $g\,L^{-1}$ in water and DMSO respectively). This solvent mixture allowed NaCl to diffuse into the initially hydrophobic gel converting it to hydrophilic via ion exchange. Once the gel is hydrophilic, the NaCl water:DMSO solution continues to enter the gel, supplying NaCl to the propagating RD front. A sharp propagating front can be readily observed under optical microscopy (because the solvent content, and thus refractive index of the gel film changes upon anion exchange (Figure 3cii). The diffusional front moves 85 μm, 140 μm and 200 μm after 5, 10 and 20 min, respectively. A similar behavior is observed for a 1:3 H2O:DMSO supporting solvent. However, what appears to be a DMSO solvation front was seen in front of the propagating gradient for this solvent system, which was not seen for the 1:1 water:DMSO solvent. Pure DMSO was not used as a solvent since the solubility of NaCl in DMSO is only 4 $g\,L^{-1}$, below that required to prepare a 2 M NaCl solution (116.88 g NaCl per L).

The impact of the dynamic gradient on transport and concentration of pyrene, a neutral non-polar fluorescent molecule, is investigated (pyrene is selected as it is hydrophobic and enables direct visualization of the propagating gradient). The gel is first dosed with pyrene by using an atomizer by spraying a 0.1 mM pyrene solution in toluene on a dry PMTA($ClO_4^-$) film and the toluene is allowed to evaporate. A PDMS block containing a microchannel is interfaced with the gel and the microchannel was filled with a 2 M NaCl (1:1) water:DMSO solution, triggering the propagating gradient (Figure 4a). The microchannel is omega-shaped, with a diameter of 500 μm (Supporting Information Section 3.1) forming a radial focusing gradient (Figure S1c). Fluorescence and brightfield images are taken at increasing times. Before triggering, pyrene is uniformly distributed across the gel (Figure 4a). Immediately after introduction of the NaCl solution into the micro-channel, a propagating gradient appears due to the conversion of the gel from hydrophobic to hydrophilic and the gradient propagates towards the center of the omega, carrying pyrene with it, and concentrating the pyrene to a small region

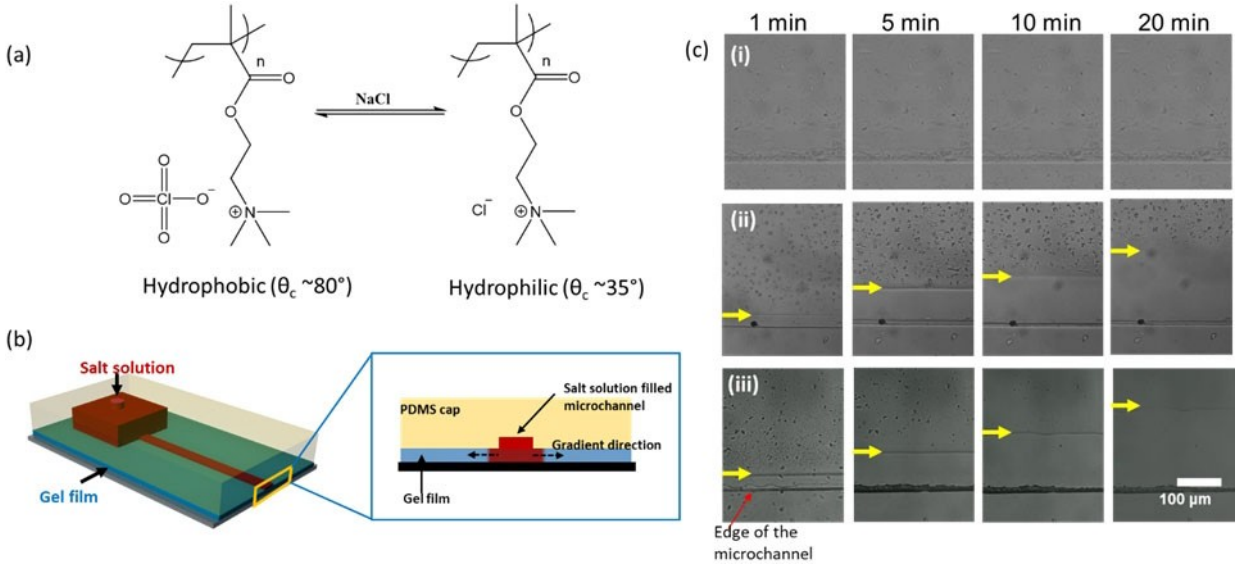


***Figure 3.*** Propagating chemical wave formation in PMTA gel films. a) Chemistries of the gel, whose hydrophobicity can be tuned by exchanging counter ion. b) Schematic diagram of a microchannel setup for the initiation propagating gradient in gel films. c) Optical images of gel film taken at various times during the propagation of the chemical wave. 2 M NaCl in the following water:DMSO ratios were injected into the microchannel, (i) $H_2O$, (ii) 1:1 water:DMSO, (iii) 1:3 water:DMSO. Yellow arrows are a guide to the eye to indicate the position of the travelling wave at the different times.

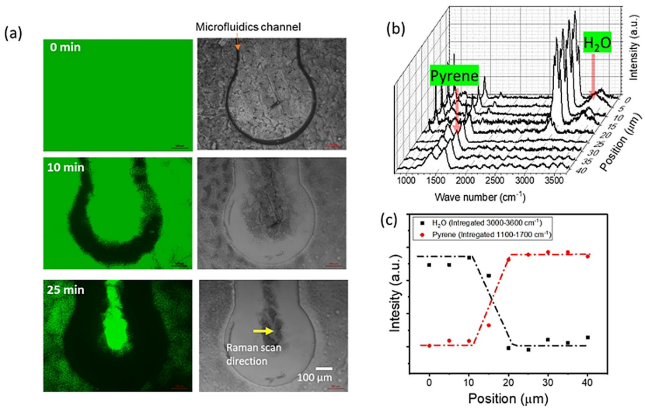


***Figure 4.*** a) Fluorescence and bright field images taken during the directed concentration of pyrene. A 2 M NaCl 1 : 1 water:DMSO solution was injected into an omega-shaped focusing microfluidic channel. b) Raman spectra across the propagating front. c) Integrated Raman peak intensity for $H_2O$ and pyrene across the propagating front.

(Figure 4a). Observed in the fluorescence images is that as gradient propagates the fluorescent intensity of the pyrene significantly increases ahead of the gradient and decreases behind the gradient. After 25 min, as the propagating gradients converge, a significant increase in fluorescence intensity is observed at the center of the omega.

To quantify dye concentration behind and front of the propagating gradient, a Raman line scan is done along the gradient after 25 min (scan line is shown in Figure 4a with yellow arrow). We note, Raman is more quantitative than fluorescence, as dye self-quenching could occur. Figure 4b shows two broad peaks around at 1363 cm$^{-1}$ and 1600 cm$^{-1}$ front of the gradient. These are the indicative of crystalline pyrene (see Supporting Information 7.4). A negligible amount of dye was found behind the gradient. Behind the gradient, a broad peak from $\nu$(O–H) at 3400 cm$^{-1}$ is observed suggesting that after ion-exchange the gel becomes hydrophilic and absorbs water. The Raman peak intensity for $\nu$(O–H) and pyrene the propagating front was integrated and plotted against the scan direction (Figure 4c). It is found that the length of the gradient is 10 µm. Using COMSOL Multiphysics® Modeling Software, the gradient position is found to be good agreement with the experimental results. Details of the COMSOL modeling can be found in the Supporting Information 7.5.

In summary, we demonstrate transportation and concentration of neutral molecules within solvent-swollen cross-linked polymer films. Two different strategies (static and dynamic gradients) are demonstrated to transport and concentrate different classes of neutral molecules. The static gradient is useful to induce movement of neutral molecules which have attractive interactions with the chemical gradient while the dynamic gradient (a "travelling wave") can drive neutral molecules, which do not have any affinity for the chemical gradient.

## Acknowledgements

This work was supported by the U.S. Department of Energy, Office of Basic Energy Sciences, Division of Materials Sciences and Engineering under Award # DE-SC0020858.

## Conflict of Interest

The authors declare no conflict of interest.

## Data Availability Statement

The data that support the findings of this study are available from the corresponding author upon reasonable request.

**Keywords:** Anisotropic Motion · Chemical Concentration and Separation · Molecular Taxi · Nano- and Micro-Machine · Stimuli Responsive Gel

[1] a) I. Prigogine, *Science* **1978**, *201*, 777–785; b) P. J. M. Van Haastert, P. N. Devreotes, *Nat. Rev. Mol. Cell Biol.* **2004**, *5*, 626–634; c) K. J. Verhey, J. W. Hammond, *Nat. Rev. Mol. Cell Biol.* **2009**, *10*, 765–777.
[2] P. Stommer, H. Kiefer, E. Kopperger, M. N. Honemann, M. Kube, F. C. Simmel, R. R. Netz, H. Dietz, *Nat. Commun.* **2021**, *12*, 4393.
[3] R. Guha, F. Mohajerani, M. Collins, S. Ghosh, A. Sen, D. Velegol, *J. Am. Chem. Soc.* **2017**, *139*, 15588–15591.
[4] a) T. H. Tsai, M. A. Ali, Z. L. Jiang, P. V. Braun, *Angew. Chem. Int. Ed.* **2017**, *56*, 5001–5006; *Angew. Chem.* **2017**, *129*, 5083–5088; b) S. Y. Zhang, S. J. Kieffer, C. J. Zhang, A. G. Alleyne, P. V. Braun, *Adv. Mater.* **2018**, *30*, 1803140; c) S. Y. Zhang, C. J. Zhang, H. Chen, S. J. Kieffer, F. Neubrech, H. Giessen, A. G. Alleyne, P. V. Braun, *Angew. Chem. Int. Ed.* **2019**, *58*, 18165–18170; *Angew. Chem.* **2019**, *131*, 18333–18338; d) C. J. Zhang, A. Sitt, H. J. Koo, K. V. Waynant, H. Hess, B. D. Pate, P. V. Braun, *J. Am. Chem. Soc.* **2015**, *137*, 5066–5073.
[5] R. Veneziano, S. Ratanalert, K. M. Zhang, F. Zhang, H. Yan, W. Chiu, M. Bathe, *Science* **2016**, *352*, 1534.
[6] M. Mathesh, J. W. Sun, F. Van der Sandt, D. A. Wilson, *Nanoscale* **2020**, *12*, 22495–22501.
[7] M. A. Ali, T. H. Tsai, P. V. Braun, *ACS Omega* **2018**, *3*, 14665–14670.
[8] a) B. K. Brandley, R. L. Schnaar, *Dev. Biol.* **1989**, *135*, 74–86; b) M. K. Chaudhury, G. M. Whitesides, *Science* **1992**, *256*, 1539–1541; c) K. Ichimura, S. K. Oh, M. Nakagawa, *Science* **2000**, *288*, 1624–1626; d) S. Daniel, M. K. Chaudhury, J. C. Chen, *Science* **2001**, *291*, 633–636; e) J. T. Smith, J. K. Tomfohr, M. C. Wells, T. P. Beebe, T. B. Kepler, W. M. Reichert, *Langmuir* **2004**, *20*, 8279–8286; f) T. M. Keenan, A. Folch, *Lab Chip* **2008**, *8*, 34–57; g) D. Ishii, M. Shimomura, *Chem. Mater.* **2013**, *25*, 509–513.
[9] R. Walder, A. Honciuc, D. K. Schwartz, *Langmuir* **2010**, *26*, 1501–1503.
[10] T. Chang, D. I. Rozkiewicz, B. J. Ravoo, E. W. Meijer, D. N. Reinhoudt, *Nano Lett.* **2007**, *7*, 978–980.
[11] P. Burgos, Z. Y. Zhang, R. Golestanian, G. J. Leggett, M. Geoghegan, *ACS Nano* **2009**, *3*, 3235–3243.

[12] A. Perl, A. Gomez-Casado, D. Thompson, H. H. Dam, P. Jonkheijm, D. N. Reinhoudt, J. Huskens, *Nat. Chem.* **2011**, *3*, 317–322.
[13] H. Chen, S. Y. Zhang, K. A. Miller, P. V. Braun, *ACS Appl. Polym. Mater.* **2020**, *2*, 3929–3935.
[14] B. Yu, C. C. Pletka, J. Iwahara, *J. Phys. Chem. B* **2020**, *124*, 1065–1070.
[15] M. Eberhardt, R. Mruk, R. Zentel, P. Theato, *Eur. Polym. J.* **2005**, *41*, 1569–1575.
[16] M. K. Gupta, R. Bansil, *J. Polym. Sci. Polym. Phys. Ed.* **1981**, *19*, 353–360.
[17] a) P. Müller, K. W. Rogers, B. M. Jordan, J. S. Lee, D. Robson, S. Ramanathan, A. F. Schier, *Science* **2012**, *336*, 721–724; b) B. A. Grzybowski, K. J. M. Bishop, C. J. Campbell, M. Fialkowski, S. K. Smoukov, *Soft Matter* **2005**, *1*, 114–128; c) E. A. Newman, K. R. Zahs, *Science* **1997**, *275*, 844–847.
[18] O. Azzaroni, A. A. Brown, W. T. S. Huck, *Adv. Mater.* **2007**, *19*, 151–154.
[19] a) M. C. Gurau, S. M. Lim, E. T. Castellana, F. Albertorio, S. Kataoka, P. S. Cremer, *J. Am. Chem. Soc.* **2004**, *126*, 10522–10523; b) Y. J. Zhang, P. S. Cremer, *Curr. Opin. Chem. Biol.* **2006**, *10*, 658–663; c) D. F. Parsons, M. Bostrom, P. Lo Nostro, B. W. Ninham, *Phys. Chem. Chem. Phys.* **2011**, *13*, 12352–12367.

Manuscript received: April 25, 2022
Accepted manuscript online: August 28, 2022
Version of record online: September 8, 2022